Astron. Astrophys. 323, 243–249 (1997)

ASTRONOMY
AND
ASTROPHYSICS

The Ar/Ca relative abundance in solar coronal plasma

P.R. Young[1], **H.E. Mason**[1], **F.P. Keenan**[2], **and K.G. Widing**[3]

[1] Department of Applied Mathematics and Theoretical Physics, Silver Street, Cambridge CB3 9EW, UK
[2] Department of Pure and Applied Physics, The Queen's University of Belfast, Belfast BT7 1NN, UK
[3] E.O. Hulburt Center for Space Research, Naval Research Laboratory, Code 7674L, Washington DC 20375, USA

Received 8 August 1996 / Accepted 29 October 1996

Abstract. The relative abundances of elements with low and high first ionisation potentials (FIP) is a subject of much recent debate. In situ measurements of the solar wind reveal a clear pattern of low FIP enhancement that has been followed up with various spectroscopic measurements of the solar corona.

Argon is unique amongst the more abundant high FIP elements in retaining several of its electrons at the high temperatures seen in flares. This allows emission lines of different ions to be compared with more confidence than for, say, hydrogen-like high FIP ions such as O VIII and Ne X.

In this paper we look at emission lines of the boron-like ion Ar XIV; in particular, the optical line at 4412 Å, seen in eclipse observations, is compared to the Ca XIII 4086 Å and Ca XV 5445 Å & 5694 Å lines to yield an Ar/Ca abundance of 0.85 ± 0.20. In the extreme ultra-violet (EUV), the Ar XIV lines at 187.94 Å and 194.41 Å can be compared with Ca XIV 193.87 Å—flare data from Skylab giving values of 1.10 ± 0.25 and 0.55 ± 0.21. Analysis of previous work indicates a photospheric Ar/Ca abundance of 1.31 ± 0.30, hence supporting the conclusion that elements with high FIP have lower coronal abundances.

Key words: Sun: abundances – Sun: corona – Sun: UV radiation

1. Introduction

Studies of optical and extreme ultra-violet (EUV) spectra of the solar corona have, for many years, suggested that the photospheric abundances of the elements are not propagated up into the corona, but instead some elements are found in greater numbers relative to others. Collecting together the different sets of analyses performed on this data, researchers have come to the broad conclusion that elements with low[1] *first ionisation potential* (or FIP) have greater abundances than those with a high FIP—see reviews by Meyer (1985a,b) and Feldman (1992).

Send offprint requests to: P.R. Young

[1] The division between low and high FIP varies but is generally taken as around 10 eV, i.e., near sulphur.

In order for the FIP to play a role in the fractionation of the elements, it is necessary to look near the temperature minimum region of the chromosphere where the high FIP elements will be neutral and so free from the effects of electric and magnetic fields. A scenario can then be envisaged whereby the charged low FIP particles are preferentially raised into the corona. A review of current thinking on the causes of the so-called 'FIP–effect' is provided by Hénoux (1995).

Argon is the only high-FIP element of significant abundance to retain several of its outer electrons at high temperatures (log $T_e \approx 6.5$), whereas elements such as Ne and O are stripped down to H and He-like states. Although these latter ions can still be used for abundance analysis (see, e.g., Schmelz 1995), problems are encountered with the large width of H and He-like ionisation fraction curves, which sample a broad range of temperatures and, potentially, coronal structures. B, C, N and O-like ions have narrower ionisation curves and so these problems are reduced. In the following analysis, we use Ar XIV (B-like), Ca XV (C-like), Ca XIV (N-like) and Ca XIII (O-like) emission features. The ionisation curves for these ions are shown in Fig. 1, and for comparison we also show those of the hydrogen-like ions O VIII and Ne X.

A hindrance with using argon for FIP-effect analysis is the uncertainty in the photospheric/solar system abundance of argon. Argon, like the other Noble gases, has large first excitation and first ionisation potentials. This has three consequences: (i), it is difficult to excite any lines of Ar I and so none are seen in photospheric spectra; (ii), Ar II, which is easier to excite, can not be formed in the Sun's photosphere; and (iii), argon is very inert and so absent in meteorites due to its reluctance to react with other elements. As it is by the study of C1 carbonaceous chondrite meteorites and the comparison of theoretical photospheric spectra with observations that the most accurate abundance determinations are achieved, other methods have to be used. We first summarise these methods in Sect. 2, and present an estimated absolute photospheric argon abundance; and then in Sects. 4 and 5 we use this as a basis to look for evidence of the FIP effect in optical and EUV coronal data. The atomic data used are summarised in Sect. 3.

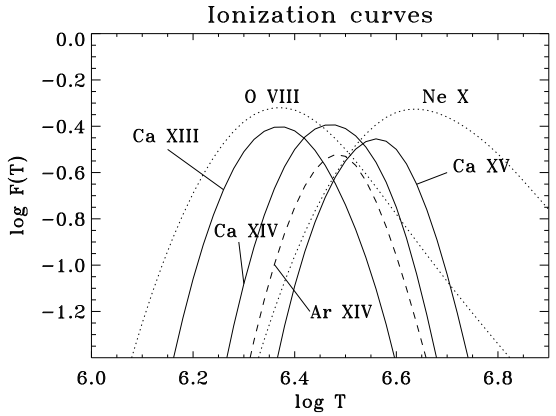

Fig. 1. Ionisation balance curves for Ca XIII–XV and Ar XIV derived from the data of Arnaud & Rothenflug (1985). The curves for the Hydrogen-like ions O VIII and Ne X are also shown to illustrate the disadvantages of using such ions.

2. Summary of previous abundance determinations

2.1. Solar X-ray data

Veck & Parkinson (1981) studied line-to-continuum ratios in data from OSO-8 and derived abundances for several coronal ions, including argon. The Ar XVII lines at 4.00 Å were used, while the continuum was fitted assuming two isothermal components due to an active region and a flare. The scatter in the data is large and an argon abundance of $6.38^{+0.18}_{-0.30}$ was derived.[2]

None of the four Bragg Crystal Spectrometers (BCS) flown on the Solar Maximum Mission (SMM) covered the 4.0 Å region, but Ar XVII lines were occasionally seen in the 3.14–3.24 Å bandpass. Doschek et al. (1985) used these lines together with the strong Ca XIX line seen at 3.177 Å to derive a coronal argon-to-calcium abundance of 0.65 ± 0.16.

Although four BCSs are currently on board the Yohkoh satellite, the wavelength coverage is such that, although the prime Ca XIX 3.177 Å line can be seen, the Ar XVII lines can not.

2.2. Solar UV emission lines

In the transition region, the dominant ionisation stages of argon are Ar V–VII, for which there exist lines in the 300–600 Å region. Feldman & Widing (1990) used some of these lines to derive an emission measure for argon which was then compared with the emission measure obtained for neon ions formed at a similar temperature, yielding an argon-to-neon abundance of 0.041 ± 0.014.

By using similarly derived Ne/Mg and Ca/Mg abundance ratios, an Ar/Ca ratio of 1.5 ± 0.8 could be estimated. This was cited as evidence of photospheric abundances in impulsive flares.

Since the completion of this work, an improved collision strength of 7.55 (compared to 5.2) for the electron excitation of the Ar VII 585.75 Å line has become available (Pradhan 1988), reducing the derived emission measure by 31%. This brings it nearer to the values for Ar V and Ar VI. From overlap of the argon ions with those of neon, the Ar/Ne abundance ratio is changed to 0.030. The neon abundance also has been updated from a study of emerging flux regions which gives a neon abundance of 8.09 ± 0.07 compared to 8.14 in the impulsive flare. Adopting the mean value of 8.11 and Ar/Ne = 0.03 the argon abundance is then 6.59 ± 0.12, with the Ar/Ca ratio falling to 1.1.

The quiet corona ($1-2\times10^6$ K) is characterised by emission from Ar IX–XI, however, as Feldman (1992) has noted, lines from Ar IX occur in the rarely observed <50Å region, while lines from Ar X and Ar XI are often rather faint. The active corona ($2-5\times10^6$ K) shows, in general, enhanced emission due to higher densities and thus the prospect of stronger lines.

2.3. Solar wind and energetic particles

Grevesse et al. (1992) give values of the argon abundance as derived from solar energetic particle (SEP) and solar wind (SW) analyses of 6.46 ± 0.06 and 6.47 ± 0.10, respectively. The former observation comes from data obtained by the Voyager 1 & 2 spacecraft (Breneman & Stone 1985), from which the argon-to-calcium abundance ratio can be derived as 0.30 ± 0.07. The solar wind data comes from an amalgam of previous results given by von Steiger & Geiss (1989) for which the calcium data is unavailable.

Although the SWICS instrument on board Ulysses has produced excellent new data for solar wind abundances, argon has been difficult to detect, while calcium is hidden amongst the stronger iron peaks (von Steiger, private communication). The triple sensors to be flown on the SMS and CELIAS experiments on the Wind and SOHO missions are expected to have sensitivities one-and-a-half orders of magnitude better than SWICS, and so should provide improved data.

2.4. Other abundance determinations

Although argon lines are not seen in the photospheric spectrum of the Sun, stars with hotter photospheres show weak absorption lines of Ar II. An analysis of the Ar II 4590 and 4658 Å lines from B-type stars in the solar neighbourhood was undertaken by Keenan et al. (1990) who gave a value of 6.49 ± 0.10. This should be a good indicator of the solar photospheric abundance of argon.

Analysis of lunar soils (Cerutti 1974) yielded an Ar/O ratio of 0.004 ± 0.001. We note that taking the photospheric oxygen abundance proposed by Grevesse et al. (1992) of 8.87 ± 0.07, would thus imply an argon abundance of 6.47 ± 0.10.

The abundance of calcium is most accurately obtained from photospheric spectra and meteorites, which give values of 6.34 ± 0.03 and 6.36 ± 0.02, respectively.

[2] The abundance notation used here is logarithmic and assumes that hydrogen has an abundance of 12.0, hence, in this case, an argon abundance of 6.38 means that argon is $6.38 - 12.00 = -5.62$ orders of magnitude less abundant than Hydrogen.

2.5. Summary

We propose here that the photospheric abundance of argon be taken as 6.47 ± 0.10[3], and thus if we take a calcium abundance of 6.35 ± 0.03 then we have an Ar/Ca abundance ratio of 1.31 ± 0.30.

The X-ray, SEP and SW data suggest that the Ar/Ca ratio is reduced to 0.30–0.60 in the corona and solar wind, and so we look to see evidence of this in the data looked at here.

3. Atomic data used in present analysis

Emission lines of Ca XIII–XV and Ar XIV are used in this paper and for each of these the most recent published atomic data are used.

For Ca XIII this means the data of Mason (1975a) were adopted, although we note that a comparison was made with some, more recent, unpublished data of A. K. Bhatia, and good agreement was found. Ca XIV, XV and Ar XIV have been assessed as part of the *CHIANTI* project (Dere et al. 1996). This involved taking published tables of collision strengths or thermally-averaged collision strengths and fitting them via the procedures described in Burgess & Tully (1992).

For Ca XIV, collision strengths and transition probabilities were taken from Bhatia & Mason (1980). Thermally-averaged collision strengths of Aggarwal et al. (1991) were used for Ca XV, together with the transition probabilities of Froese Fischer & Saha (1985) and, for the ground levels, the proton collision rates of Faucher (1977).

Recent work on the boron sequence by Zhang et al. (1994) gave thermally-averaged collision strengths for Ar XIV, while transition probabilities were obtained from Dere et al. (1979) and Bhatia et al. (1986). The proton rates of Foster et al. (1996) were used for the ground transition.

For the optical lines seen in the eclipse data, it is important to allow for photo-excitation by the background photospheric radiation field. The observations were made approximately 0.15 $R_\odot$ above the limb, so a dilution factor of 0.3 was used.

For the interpretation of the eclipse data the ionisation balance calculations of Arnaud & Rothenflug (1985) were used.

4. Ground-based observations of coronal argon lines

Ar XIV 4412 Å is the only useful 'high FIP line' from the corona that is accessible to ground-based observers and, even then, it is only seen during flares or coronal condensations due to the high temperature of maximum ionisation, $T_{\max}$, of Ar XIV (3.0×10^6 K).

[3] Grevesse et al. (1992) revised the value given by Anders & Grevesse (1989) of 6.56 ± 0.10 to 6.53 ± 0.10 based on SW and SEP measurements together with the Feldman & Widing (1990) EUV result. Essentially we are neglecting the latter measurement and taking into account the B-type stars and lunar soil work, which are consistent with the SW and SEP results. With the new atomic data mentioned in Sect. 2.2, the Feldman & Widing result becomes closer to our value, giving added confidence in the result given here.

Calcium is a useful element with which to compare argon regarding the FIP effect, on account of its low FIP, and the fact that they have similar abundances so that their line intensities have a similar order of magnitude. Of the calcium ions, Ca XIV has a $T_{\max}$ of 2.8×10^6 K making it the ideal ion to compare with Ar XIV, however Ca XIV does not emit any lines in the visible. We do, however, find prominent lines from Ca XIII and Ca XV at 4086 Å and 5694 Å in the visible; indeed the former line was used by Zirin (1964; see also Zirin 1988) to derive an estimate of the Ar/Ca relative abundance in a post-flare condensation of 0.5.

The differences in $T_{\max}$ of the Ar XIV, Ca XIII and Ca XV ions shown in Fig. 1 mean one has to be careful in directly comparing any two lines from these ions. Instead one can use the Ca XIII and Ca XV lines to interpolate what the temperature structure is like over the range occupied by Ar XIV and then derive the Ar/Ca relative abundance. This is the technique used here and the details of the theory are given below in Sect. 4.2, but first we describe the observational data that was used.

4.1. The 1952 eclipse data

Perhaps the best observation of the argon and calcium lines in the literature is the data obtained by B. Lyot and M. K. Aly at the total solar eclipse observed at Khartoum on February 25, 1952, and reported by Aly et al. (1962). Fig. 7 of this work shows the variation of line intensities from the Ar XIV, Ca XIII and Ca XV lines mentioned above across a coronal condensation. In addition we can also see the Ca XV 5445 Å line. We will proceed to use all four of these lines to estimate the Ar/Ca relative abundance in the condensation.

Aly et al. do not give numerical values for the variation of intensity across the condensation, only graphs. Thus in Table 1 we give the intensities derived from these graphs. Note that only eight locations across the condensation are studied here—locations 3–5 correspond to the core of the condensation.

4.2. Theory

The theoretical intensity for a line λ of some ion is given by

$$I_{\rm th}(\lambda, T) \propto \epsilon(\lambda).\mathscr{F}(T).\mathscr{A},$$

where $\mathscr{F}(T)$ is the ionisation fraction of the ion, $\mathscr{A}$ the element abundance, and $\epsilon(\lambda)$ the emissivity of the line, given by

$$\epsilon(\lambda) \propto \frac{A_\lambda N(T, N_e)}{\lambda}, \quad (1)$$

where A_λ is the transition probability for the transition giving rise to the line at wavelength λ, and N is the occupation number for the atomic level emitting the line.

N varies with both the electron number density, $N_{\rm e}$, and the temperature, T. However, N varies slowly with T in relation to $\mathscr{F}(T)$ and it will be assumed that the emitting region is at a fixed density (see Sect. 4.3), so we take only the values of $\epsilon(\lambda)$ at that density and the $T_{\max}$ of the ion.

Table 1. Observed intensities for 8 locations across the condensation

Ion	Line (Å)	1	2	3	4	5	6	7	8
Ca XV	5694	11.9	17.9	24.0	27.6	26.8	16.6	11.0	9.4
	5445	-	-	8.4	14.8	11.8	-	-	-
Ar XIV	4412	5.1	7.4	18.6	21.1	15.6	12.7	8.9	7.0
Ca XIII	4086[a]	4.3	8.5	12.5	16.6	20.6	18.8	11.0	10.5

[a] There is a contribution to this line from material in-front-of and behind the condensation, which has been subtracted.

Table 2. Derived values of m and $\mathscr{A}(Ar)/\mathscr{A}(Ca)$ for each of the 8 locations across the condensation.

Quantity	1	2	3	4	5	6	7	8
$I_{\rm obs}$(4086 Å)/$I_{\rm obs}$(5694 Å)	0.36	0.47	0.52	0.60	0.77	1.13	1.00	1.12
m	0.38	-0.30	-0.53	-0.88	-1.47	-2.39	-2.09	-2.34
$I_{\rm obs}$(4412 Å)/$I_{\rm obs}$(5694 Å)	0.43	0.41	0.78	0.76	0.58	0.77	0.81	0.74
$\mathscr{A}(Ar)/\mathscr{A}(Ca)$	0.63	0.54	0.99	0.91	0.63	0.73	0.80	0.70

To calculate ϵ, the level balance equations for the ion need to be solved. The atomic processes included in these calculations were electron and proton excitation and de-excitation, together with radiative decay. The atomic data for these processes has been described in Sect. 3.

$I_{\rm th}(\lambda, T)$ only tells us the radiation emitted by some unit amount of plasma at a temperature T. In reality, we will have plasma distributed over a range of temperatures, the amount of plasma at any given temperature being specified by the emission measure $\mathscr{E}(T)$, and so the observed intensity of the line λ is given by

$$I_{\rm obs}(\lambda) \propto \int_{\Delta T} I_{\rm th}(\lambda, T)\mathscr{E}(T)dT$$

where I_{obs} is the observed intensity and ΔT is the temperature region where the ion is found (determined by the ionisation balance calculations). Hence

$$I_{\rm obs}(\lambda) \propto \epsilon(\lambda).\mathscr{A} \int_{\Delta T} \mathscr{F}(T)\mathscr{E}(T)dT.$$

Since the three ions considered here are formed in a narrow temperature region (see Fig. 1), we assume the simple relation

$$\log \mathscr{E}(T) \propto m \log T$$

(This follows from the standard practice of plotting $\log \mathscr{E}$ against $\log T$, which typically gives a slowly-varying curve.)

The ionisation fraction is often tabulated as $\log.\mathscr{F}$ against $\log T$, and so it is convenient to define

$$\xi(t) = \log.\mathscr{F}(t) + \log \mathscr{E}(t) + t$$

for $t = \log T$, giving

$$I_{\rm obs}(\lambda) \propto \epsilon(\lambda).\mathscr{A} \int_{\Delta t} 10^{\,\xi(t)} dt$$

If we break Δt into n intervals of width 0.02 dex over each of which we approximate ξ by a straight line, then

$$I_{\rm obs}(\lambda) \propto \epsilon(\lambda).\mathscr{A}.\mathscr{S}(m) \tag{2}$$

where, for a given ion,

$$.\mathscr{S}(m) = \sum_{i=1}^{n} \frac{10^{a_i t_i + b_i}(10^{a_i 0.02} - 1)}{a_i \ln 10}$$

and $\xi(t) = a_i t + b_i$ in the interval $[t_i, t_{i+1}]$.

Our recipe for determining the Ar/Ca relative abundance is then as follows:

1. The Ca XV lines at 5445 Å and 5694 Å are density sensitive—see, e.g., Mason (1975a)—and so we can determine the electron density, $N_{\rm e}$, and thus from Eq. (1) determine the emissivities, ϵ, of all the lines.

2. The Ca XIII and Ca XV lines are formed at different temperatures, bracketing the Ar XIV line (see Fig. 1) and so comparing these lines enables the slope m of the emission measure curve to be determined. We have, from Eq. (2),

$$\frac{I_{\rm obs}(4086\ \text{Å})}{I_{\rm obs}(5694\ \text{Å})} = \frac{\epsilon(4086\ \text{Å})}{\epsilon(5694\ \text{Å})} \frac{.\mathscr{S}(m;\text{CaXIII})}{.\mathscr{S}(m;\text{CaXV})}, \tag{3}$$

and by an iterative process we take values of m and calculate the $.\mathscr{S}$ functions in an attempt to match the observed 4086/5694 ratio.

3. With this value of m, we can then calculate the $.\mathscr{S}$ function for the Ar XIV 4412 Å line. Taking the ratio of 4412/5694, we have, from Eq. (2),

$$\frac{I_{\rm obs}(4412\ \text{Å})}{I_{\rm obs}(5694\ \text{Å})} = \frac{.\mathscr{A}(Ar)}{.\mathscr{A}(Ca)} \frac{\epsilon(4412\ \text{Å})}{\epsilon(5694\ \text{Å})} \frac{.\mathscr{S}(m;\text{ArXIV})}{.\mathscr{S}(m;\text{CaXV})}. \tag{4}$$

Our free parameter is now the Ar/Ca relative abundance which we adjust until the right-hand-side of Eq. (4) matches the observed ratio of the two lines.

Table 3. Emissivity ratios for argon and calcium coronal ions.

	N_e(cm^{-3})		
	1×10^9	5×10^9	1×10^{10}
ϵ(4086 Å)/ϵ(5694 Å)	0.39	0.49	0.56
ϵ(4412 Å)/ϵ(5694 Å)	0.76	1.05	1.15

Table 4. The data represented in Fig. 2.

	log N_e								
Ratio	9.0	9.5	10.0	10.5	11.0	11.5	12.0	12.5	13.0
R_1	0.52	0.52	0.49	0.44	0.37	0.34	0.36	0.43	0.56
R_2	0.84	0.85	0.87	0.90	0.95	1.03	1.18	1.48	1.95

4.3. Results

As the Ca XV 5445 Å line was only recorded for three locations in the centre of the condensation (Table 1) we summed the three intensities and those of the 5694 Å line; the 5445/5694 ratio was then 0.45, which from our line ratio calculations implied an electron density of 5×10^9 cm^{-3}. In Table 3 we show the values of the two emissivity ratios in Eqs. (3) and (4) at this density together with the values at 10^9 cm^{-3} and 10^{10} cm^{-3}, which show the effects of differing densities.

Following the recipe of the previous section, we give the m values, derived from Eq. (3), for each of the 8 locations across the condensation in Table 2, together with the abundance ratios derived from Eq. (4).

The major sources of errors in the above analysis are as follows:

1. *The assumption of constant density.* In the analysis of the same condensation by Mason (1975b), a complex model of the structure of the condensation is proposed, but essentially the density is considered to decrease away from the centre. Thus we may expect the density to fall away from the central locations where the calcium lines are strongest. As the emissivity of the argon line falls most rapidly with density, a density lower than 5×10^9 cm^{-3} would imply a *higher* Ar/Ca abundance than that given in Table 3, which would make the abundances at these locations more in line with those at the central locations. Conversely, a higher density would imply a lower Ar/Ca abundance.

2. *The position of the argon ionisation curve relative to those of the calcium ions, and their relative heights.* The ionisation balance calculations of Arnaud & Rothenflug (1985) are by no means definitive—for example density effects in dielectronic recombination are not included—and thus this is one of the major sources of uncertainty. We estimate the likely errors will be around $\pm$20%.

Given the above discussion of errors, we feel that the argon-to-calcium abundance ratio implied by the eclipse data be taken as 0.85 ± 0.20.

5. EUV line abundance determination

Unlike the optical data, we have lines from several consecutive ionisation stages of argon and calcium in the EUV—early work by Purcell & Widing (1972) identified many lines from the stages Ar XII–XVI and Ca XIV–XVIII in a flare. We will concentrate here only on the Ar XIV 187.94 Å and 194.41 Å, and Ca XIV 193.87 Å lines, whose proximity in wavelength facilitates a study of the Ar/Ca relative abundance. The ratios to be studied are:

R_1 = 194.41/193.87

R_2 = (187.94 + 194.41)/193.87

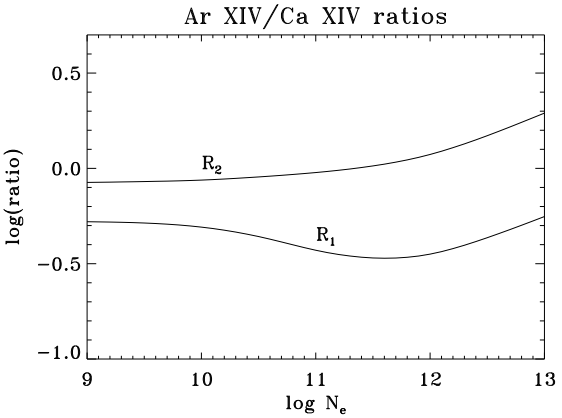

Fig. 2. The variation of Ar XIV/Ca XIV line ratios with electron density, assuming a 'flat' emission measure curve and an Ar/Ca abundance ratio of 1.

By virtue of the similar values of T_{max} for Ar XIV and Ca XIV (see Fig. 1), we are not concerned about the effects of a slope in the emission measure curve on the predicted intensities of the argon and calcium lines here. Instead we will assume a zero-gradient emission measure curve—the errors incurred by this will be discussed later.

Fig. 2 and Table 4 show how the R_1 and R_2 ratios vary with density *assuming* the lines are emitted by a plasma with a zero-gradient emission measure curve *and* that the Ar/Ca abundance ratio is 1. Clearly, neither ratio is completely density insensitive but we note that, below 10^{12} cm^{-3}, R_2 is the least sensitive. Also, the 194.41 line is relatively weak which would make results using only this line more uncertain.

5.1. Observations

The only instrument that has observed the Ar XIV and Ca XIV lines to date is the Naval Research Laboratory's slitless objective grating spectroheliograph (S082A) on board *Skylab* (although the CDS unit on SOHO should also see them—see Sect. 6). The lines we are interested in are only seen in high temperature, flaring regions and even then are fairly weak.

Table 5. Ar XIV and Ca XIV relative line intensities from the SO82A instrument on Skylab.

		Ar XIV		Ca XIV
Plate	Observing time	187.94	194.41	193.87
3A-133	17 Dec 1973 00:45:19	0.17	0.10	0.51
3A-465	21 Jan 1974 23:24:24	0.64	0.28	0.67
3A-466	21 Jan 1974 23:27:39	0.66	0.33	0.99

Table 6. Results for the Skylab data.

Plate	R_2	Density	Abundance
3A-133	0.53 ± 0.21	11.1 ± 0.5	0.55 ± 0.21
3A-465,466	1.15 ± 0.25	11.6 ± 0.4	1.10 ± 0.25

The solar images produced by S082A overlapped, and so it is most appropriate to study small, flaring 'kernels' when looking for features in weaker lines. Two of the best examples were flares seen on 17 Dec 1973 and 21 Jan 1974. Detailed studies of these flares are presented in Widing & Spicer (1980) and Widing & Hiei (1984), respectively. In both cases the flares were interpreted as being associated with the emergence of magnetic flux into the solar atmosphere.

The best quality data for the flares were found on plates 3A-133, 3A-465 and 3A-466. The relevant line intensities are given in Table 5.

5.2. Results

Table 6 shows the results derived from the SO82A data. We have summed together the observations for the Jan 21 flare as the data were taken in quick succession and so one would not expect the physical conditions to change significantly in this time.

The electron densities given in Table 6 were derived from the 187.94/194.41 Ar XIV ratio, which is density sensitive between 10^{10} and 10^{12} cm^{-3}—see Keenan et al. (1996).

The most significant likely errors in the abundances are:

1. *Measuring errors (photon statistics, fitting errors).* These errors are taken as 25% for plates 3A-465,466 and 40% for plate 3A-133 (Widing, unpublished data), for the argon-to-calcium ratios.

2. *Errors in the density estimate lead to uncertainties in estimating the theoretical ratio (see Table 4 and Fig. 2).* Of principal concern is whether the density in either of the flares may have exceeded 10^{12} cm^{-3}, above which R_2 becomes strongly density sensitive. For this purpose we cite the Ca XV line ratios of Keenan et al. (1988), who give densities of $10^{11.1-11.2}$ cm^{-3} for the two flares above, thus giving us confidence in the densities given here.

5.3. Discussion

The data show that the Jan 21 flare has an Ar/Ca abundance roughly in agreement with the photospheric values given in Sect. 2.6, but that the Dec 17 flare clearly has an Ar/Ca abundance around one half of the photospheric abundance. We note that while the Ca XIV line is of a similar order of magnitude in the two flares (Table 5), the Ar XIV lines are clearly weaker in the Dec 17 flare.

This is not a density effect as higher densities would require a lower Ar/Ca ratio, while lower densities would have little effect on the result. A steep slope in the emission measure curve may cause an anomalous abundance determination, but the curves given in Widing & Spicer (1980), and Widing & Hiei (1984) for the two flares are of a similar shape, and so we would at least expect a consistent anomaly for the two flares.

Previously it has been thought that flares associated with emerging flux show photospheric abundances (Feldman & Widing, 1990), and so our result for the Dec 17 flare is surprising.

6. Conclusion and future work

Our investigation of the argon-to-calcium abundance in the solar atmosphere has led us to the following conclusions:

1. Analysis of previous work on argon abundances yields an estimate of the photospheric/solar system abundance of 6.47 ± 0.10, while folding this with the abundance of calcium leads to a photospheric Ar/Ca abundance ratio of 1.31 ± 0.30.
2. The 1952 eclipse data give an Ar/Ca ratio of 0.85 ± 0.20 for a coronal condensation.
3. EUV line ratios for Ar XIV and Ca XIV suggest ratios of 1.10 ± 0.25 and 0.55 ± 0.21 for the Jan 21 and Dec 17 flares, respectively.

Previous studies of the FIP effect have shown varying degrees of low FIP enhancement, and this is reflected in the present analysis. The 1974 Jan 21 flare shows an Ar/Ca ratio little different from the photospheric value, while the 1973 Dec 17 flare value is around 2 to 3 times lower. The eclipse data suggests a value of around one half of the photospheric value.

The Coronal Diagnostic Spectrometer (CDS, described in Harrison et al. 1995) on board the Solar and Heliospheric Observatory (SOHO) will provide high resolution spectra in the EUV. In particular, the Grazing Incidence Spectrometer (GIS) will cover the 153–221 Å wavelength region, and thus will be capable of seeing not just the Ar XIV 187.94 Å & 194.41 Å and Ca XIV 193.87 Å lines, but also Ca XIII 156.68 Å and Ca XV 200.98 Å, which should allow a detailed analysis of the argon-to-calcium abundance. However, we note that SOHO will be observing during a quiet phase of the Sun, where high temperature plasma will be less common.

Acknowledgements. PRY and HEM acknowledge the financial support of PPARC. FPK is grateful to the Royal Society for financial support

References

Aggarwal K. M., Berrington K. A., Keenan F. P., 1991, ApJS 77, 441

Aly M. K., Evans J. W., Orrall F. Q., 1962, ApJ 136, 956
Anders E., Grevesse N., 1989, Geochim. Cosmochim. 53, 197
Arnaud M., Rothenflug R., 1985, A&AS 60, 425
Bhatia A. K., Mason H. E., 1980, MNRAS 190, 925
Bhatia A. K., Feldman U., Seely J. F., 1986, ADNDT 35, 319
Breneman H. H., Stone E. C., 1985, ApJ 299, L57
Burgess A., Tully J.A., 1992, A&A 254, 436
Cerutti H., 1974, Die Bestimmung des Argons im Sonnenwind aus Messungen an den Apollo-SWC-Folien. Dissertation, Univ. Bern
Dere K. P., Mason H. E., Widing K. G., Bhatia A.K., 1979, ApJS 40, 364
Dere K. P., Landi E., Mason H. E., Monsignori-Fossi B. M., Young P. R., 1996, A&AS *in preparation*
Doschek G. A., Feldman U., Seely J. F., 1985, MNRAS 217, 317
Faucher P., 1977, A&A 54, 589
Feldman U., 1992, Phys. Scripta 46, 202
Feldman U., Widing K. G., 1990, ApJ 363, 292
Foster V. J., Reid R. H. G., Keenan F. P., 1996, A&A *in press*
Froese Fischer C., Saha H. P., 1986, Phys. Scripta 32, 181
Grevesse N., Noels A., Sauval A. J., 1992, Photospheric Abundances. In: Proc. of the First SOHO Workshop. ESA SP-348, p. 305
Harrison R. A., Sawyer E. C., Carter M. K., et al., 1995, Sol. Phys. 162, 233
Hénoux J.-C., 1995, Adv. Space Res. 15 (7), 23
Keenan F. P., Aggarwal K. M., Berrington K. A., Widing K. G., 1988, ApJ 327, 473
Keenan F. P., Bates B., Dufton P. L., Holmgren D. E., Gilheany S., 1990, ApJ 348, 322
Keenan F. P., Foster V. J., Pradhan A. K., Zhang H. L., Widing K. G., 1996, ApJ *submitted*
Mason H. E., 1975a, MNRAS 170, 651
Mason H. E., 1975b, MNRAS 171, 119
Meyer J.-P., 1985a, ApJS 57, 151
Meyer J.-P., 1985b, ApJS 57, 172
Pradhan A. K., 1988, ADNDT 40, 335
Purcell J. D., Widing K. G., 1972, ApJ 176, 239
Schmelz J. T., 1995, Adv. Space Res. 15 (7), 77
Steiger R. von, Geiss J., 1989, A&A 225, 222
Veck N. J., Parkinson J. H., 1981, MNRAS 197,41
Widing K. G., Hiei E., 1984, ApJ 281, 426
Widing K. G., Spicer D. S., 1980, ApJ 242, 1243
Zirin H., 1964, ApJ 140, 1216
Zirin H., 1988, Astrophysics of the Sun. Cambridge Univ. Press, Cambridge, p. 233
Zhang H. L., Graziani M., Pradhan A. K., 1994, A&A 283, 319

This article was processed by the author using Springer-Verlag LaTeX A&A style file *L-AA* version 3.